



Effective removal of 17 α -ethynyl estradiol by nano-iron/multi-wall carbon nanotubes composite

Yifei Zhang^a, Hongbin Wang^a, Ting Zhao^b, Lei Liu^a, Lijun Luo^a, Wei Tan^{a,*}, Manhong Liu^{a,*}

^aKey Laboratory of Resource Clean Conversion in Ethnic Regions, School of Chemistry and Environment, Yunnan Minzu University, Kunming, Yunnan 650500, China, email: 1821157000@qq.com

^bThe First Middle School of Yiliang County, Zhaotong, Yunnan 657000, China, emails: 317366182@qq.com (W. Tan), lmh6211@126.com (M. Liu), 1762646849@qq.com (Y. Zhang), wanghb2152@126.com (H. Wang), 921583992@qq.com (L. Liu), 10501931@qq.com (L. Luo)

Received 8 May 2020; Accepted 29 September 2020

ABSTRACT

In this work, a new composite material was prepared and used to remove 17 α -ethynyl estradiol (EE2). The structure and morphology of multi-walled carbon nanotubes (MWNTS), activated multi-walled carbon nanotubes (A-MWNTS) and nano-iron/multi-wall carbon nanotubes (A-MWNTS/Fe) were characterized by transmission electron microscopy, scanning electron microscopy, X-ray photoelectron spectroscopy, and Brunauer–Emmett–Teller. The influencing aspects including equilibrium time, A-MWNTS/Fe dosage, pH, initial EE2 concentration, temperature, different materials, and interference factors on the EE2 removal were investigated. The results show that when the time is 20 min, the dosage of A-MWNTS/Fe is 0.015 g, pH is 6–8, the initial concentration of EE2 is 3 mg L⁻¹, and the temperature is within the range of 15°C–25°C, the removal rate of EE2 reach over 99%. Moreover, the adsorption data are in good agreement with the Langmuir isotherm model and the pseudo-second-order kinetic model. EE2 can be removed by A-MWNTS/Fe because of its high practicability and good application prospect, and the removal rate can reach more than 90%. In summary, A-MWNTS/Fe with facile synthesis method, efficient adsorption performance, and excellent reusability shows potential promise for the treatment of wastewater.

Keywords: Nano-iron; Activated multi-walled carbon nanotubes (A-MWNTS); EE2; Adsorption

1. Introduction

Endocrine-disrupting chemicals (EDCs), also known as environmental hormones, mainly originate from domestic sewage, industrial wastewater, and precipitation runoff [1,2]. EDCs can be absorbed by humans, animals, and plants through diet and contact [3,4]. As studies show, human beings and animals may have healthy problems due to the long-term exposure of EDCs, such as male reproductive tissue malformation, female genital tissue cancer, neurological disorders, and other hazards [5]. EE2 is an oral contraceptive with strong estrogen activity and one of the most active

EDCs [6,7]. It can spread to the human body through the biological chain, which causes the body's endocrine disorders and other more serious hazards [8–10]. Therefore, it is necessary to develop an effective process combined with wastewater treatment technology to completely remove EE2 from wastewater and discharge it into the receiving water environment [11,12].

Some studies have pointed out that the removal methods of pollutants in environmental water include chemical precipitation [13], adsorption, and membrane separation [14,15]. Adsorption has been considered as one of the most common and efficient methods because the method has

* Corresponding author.

Presented at the 12th International Conference on Challenges in Environmental Science & Engineering (CESE-2019), 3–7 November 2019, Kaohsiung, Taiwan

the advantages of simple operation, high efficiency, good selectivity, and low cost [16,17]. The main principle is that the adsorption material can effectively remove the residual refractory organic matter and trace metals after conventional sewage treatment. Therefore, the selection of adsorption materials has become a key factor in the treatment. Nano-iron is widely used in aqueous environment due to its small size, large specific surface area, and high surface energy [18]. However, nano-iron has some defects such as instability, agglomeration, oxidation, and loss of application in water, which will limit its practical application in water treatment. To solve these problems, many researchers have paid attention to the modification of nano-iron [19]. The purpose is to improve the stability, the oxidation resistance of nano-iron, and maintain its original activity. The preparation of nano-iron composite is one of the effective ways to alleviate the defects of it, and the problems of agglomeration and oxidation should be avoided in the preparation of composite [20,21]. In order to challenge the above drawbacks, it is of vital importance to select the right carriers [22,23]. Besides the characteristics of stable structure, good dispersion, and high adsorption capacity, it should also prevent oxidation of nano-iron.

Carbon nanotubes have a large surface area and a large number of active sites for adsorption, and have been used in environmental water treatment due to their unique adsorbability [24]. Yangmei et al. [25] used carbon nanotubes to adsorb four phenolic substances, including A-naphthol and nitrophenol. El-Sweify et al. [26] showed that the oxide carbon nanotubes could rapidly adsorb Sudan red, with the maximum adsorption capacity of 41.0408 and 47.037 mg g⁻¹. Yang [27] conducted adsorption studies on carbon nanotube materials such as fullerenes, single-walled carbon nanotubes, and multi-walled carbon nanotubes, and found that the adsorption performance of different polycyclic aromatic hydrocarbons was related to the molecular size, specific surface area, and micropore structure of carbon nanotubes. It can be seen that the adsorption capacity of the functionalized carbon nanotubes is significantly better than that of unactivated carbon nanotubes. Because activated multi-walled carbon nanotubes (A-MWNTS) has unique topological structure, high mechanical strength, and chemical inertness [28], this is the essential condition of nano-iron carrier [29,30].

In this work, nano-iron/multi-wall carbon nanotubes (A-MWNTS/Fe) was prepared by loaded nano-iron on A-MWNTS to improve EE2 removal efficiency. The effects of different parameters on the removal of EE2 in wastewater by A-MWNTS/Fe, the kinetics, thermodynamics of the adsorption process, the characterization of composite, and the evaluation of regeneration performance are investigated. This is of great significance for the following research on the complete removal of target pollutants.

2. Experimental

2.1. Materials

All aqueous solutions were prepared using ultrapure water. All chemicals used in this work were analytical grade. Ferric chloride (FeCl₃), potassium hydroxide (KOH),

and sodium hydroxide (NaOH) were purchased from Fengchuan Chemical Reagent Technology Co., Ltd., Tianjin, China. Potassium borohydride (KBH₄) was provided by Tianjin Damao Chemical Reagent Factory Co., Ltd., China. Anhydrous ethanol (C₂H₅OH) was bought from Xilong Chemical Co., Ltd., China. 17-ethynyl estradiol (EE2, purity 98%) was obtained from Sigma-Aldrich Co., Ltd., (Shanghai). Methanol (CH₃OH) was guaranteed reagent from American TEDIA reagent company. Multi-wall carbon nanotubes (MWNTS; Purity > 95 wt.%, OD > 50 nm) was bought from Chengdu Organic Chemicals Co., Ltd., Chinese Academy of Sciences.

2.2. Preparation of A-MWNTS/Fe

The composite A-MWNTS/Fe was successfully completed by the following main steps [31]. Firstly, 0.436 g FeCl₃ was dissolved in 30 mL ethanol/water (V ethanol/V water = 7:3) and 0.218 g A-MWNTS solution was added (KOH as activator, the ratio of alkali and carbon was 3:1, the MWNTS were activated at 850°C for 40 min after ultrasonic mixing). Then, it was transferred to a three-mouth flask of 250 mL and stirred under nitrogen for 15 min. Under the condition of rapid agitation, 15 mL of newly prepared 0.573 mol L⁻¹ of KBH₄ solution was added to the mixture at a constant speed of 10.0 mL min⁻¹ for 90 min. Thereafter, after centrifugation, the precipitate was rinsed deionized water and ethanol for three times respectively. After freeze-drying, they were dried in a vacuum drying oven, which was designated as A-MWNTS/Fe.

2.3. Detection and characterization

0.0300 g EE2 was accurately weighed in a 10.00 mL volumetric flask, and 3 g L⁻¹ EE2 reserve solution was prepared with methanol as the co-solvent at constant volume. The EE2 reserve solution was put into a refrigerator at 5°C for preservation.

EE2 was determined by high-performance liquid chromatography. The detection conditions were as follows: the column was SB-C18 reversed phase column (4.6 × 250 mm, 5 μm), the column temperature was 30°C, the injection volume was 25 μL, the mobile phase was methanol/water (volume ratio 9:1), the flow rate was 0.8 mL min⁻¹, and the ultraviolet detection wavelength was 210 nm. Under this detection condition, the retention time of EE2 was 7 min. The peak time of EE2 was about 5.6 min. As shown in Fig. 1, the linear equation of EE2 was $A = 75.848c - 3.4826$ (c is EE2 concentration, A is measured peak area) and the linear correlation coefficient was 0.9999.

The morphological structure, chemical composition, specific surface area, and pore size distribution of MWNTS, A-MWNTS, and A-MWNTS/Fe were characterized by transmission electron microscopy (TEM), X-ray photoelectron spectroscopy (XPS), and Brunauer–Emmett–Teller (BET), respectively.

2.4. Adsorption experiment

In this work, the adsorption was influenced by some important parameters encompassing initial concentration of

EE2, contact time and solution temperature, etc. Therefore, the adsorption behavior of adsorbent was discussed. The working solutions of the EE2 stock were prepared at a low temperature and kept for use. The certain amount of A-MWNTS/Fe was accurately weighed, then 100 mL of 3 g L⁻¹ EE2 solution was added, and the pH of the solution was adjusted with 1 mol L⁻¹ NaOH and HCl. After oscillating in a constant temperature oscillator for 60 min at a speed of 240 rpm at 25°C, the supernatant was passed through a 0.45 μm membrane microporous filter, and then its concentration was determined. The adsorption capacity of the adsorbent was calculated by the following equations:

$$R\% = \frac{C_0 - C_t}{C_0} \times 100\% \quad (1)$$

where C_0 (mg L⁻¹) and C_t (mg L⁻¹) are the initial, the equilibrium concentration of EE2, respectively. The R is the removal rate (%) of EE2.

The amount of EE2 adsorbed per unit mass of the adsorbent was quantified using the mass balance equation as follows:

$$q_e = \frac{V(C_0 - C_t)}{m} \quad (2)$$

where q_e is the adsorption capacity (mg g⁻¹), C_0 (mg L⁻¹) and C_t (mg L⁻¹) are the initial, the equilibrium concentration of EE2, respectively, V is the volume (L) of solution, and m is the weight (g) of adsorbent.

2.5. Regeneration experiment

The initial concentration of EE2 was 3 mg L⁻¹, the dosage of A-MWNTS/Fe was 0.015 g, and the adsorption time

was 20 min when the first adsorption experiment was conducted. After the adsorption was completed, the saturated adsorption A-MWNTS/Fe was washed by anhydrous alcohol for reuse. After seven adsorption–regeneration cycles, the adsorption performance was compared.

3. Results and discussion

3.1. Material characterization

3.1.1. Materials morphology by TEM and SEM

The microstructures of materials are indicated in TEM. Fig. 2 depicts TEM images of MWNTS, A-MWNTS, and A-MWNTS/Fe. From Figs. 2a and b, MWNTS

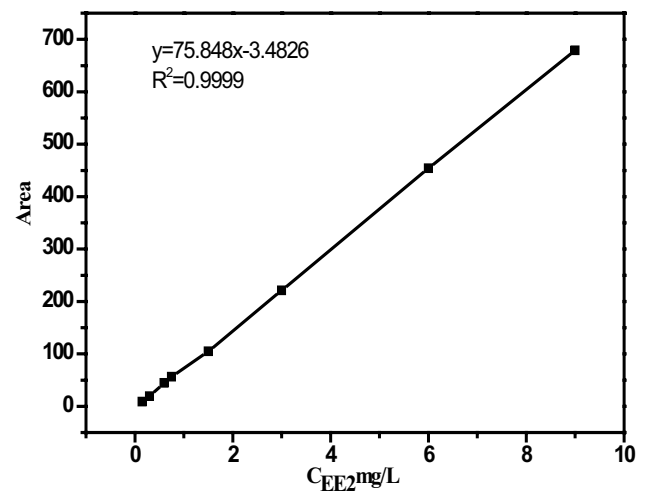


Fig. 1. EE2 standard curve.

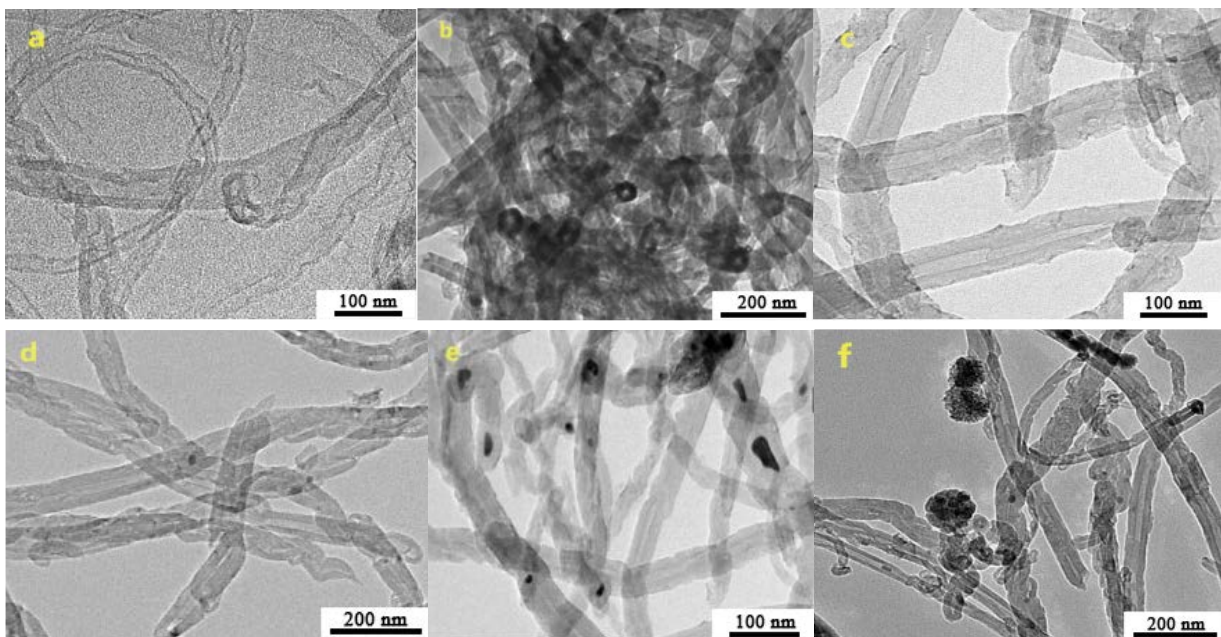


Fig. 2. TEM image of MWNTS (a and b), A-MWNTS (c and d), and A-MWNTS/Fe (e and f).

intertwine with each other and have serious agglomeration. Obviously, comparing with the original MWNTS (Figs. 2a and b), the A-MWNTS (Figs. 2c and d) are characterized with dispersed, rough surface, partial fracture, and collapse. Moreover, the specific surface area is effectively increased, which is beneficial to the loading of nano-iron [32]. It is known as Figs. 2e and f that the nano-iron is loaded on the surface of A-MWNTS in the form of particles, and a few enter the interior of A-MWNTS with irregular shapes. It can be proved that KOH can not only corrode the surface of A-MWNTS, but also open its ports to allow nano-iron to enter. The results show that nano-iron is successfully loaded on A-MWNTS, which increases the active site of A-MWNTS/Fe composites [33,34].

Fig. 3 shows the SEM scan of A-MWNTS/Fe. Comparing Fig. 3a and b, there is obvious nano-iron with a particle size of about 39 nm, which further shows that the nano-iron has been successfully loaded on A-MWNTS.

3.1.2. XPS analysis

The main elemental composition and chemical state of A-MWNTS/Fe were analyzed by XPS. The XPS full scan spectrum, Fe3p spectrum, and Fe2p spectrum of A-MWNTS/Fe before and after EE2 adsorption are shown in Fig. 4. Comparing Figs. 4a and b show that there are three elements of Fe, O, and C on the surface of the adsorbent before and after the reaction. These elements come from MWNTS, nano-iron, and nano-iron oxides in the composite materials. These further explanation that A-MWNTS and nano-iron have been successfully compounded. After adsorption, the Fe and O peaks are obviously weakened. It may be that EE2 is deposited on the nano-iron surface [35,36]. Figs. 4e and f clearly show that the binding energies of Fe2p_{3/2} and Fe2p_{1/2} are 709.5 and 723.2 eV after adsorption respectively (Fig. 4f), and the two peak heights are weaker than that before adsorption. It shows that there are a lot of Fe²⁺ and Fe³⁺ in the composite after the reaction. The satellite peak of Fe2p_{3/2} is located at 715.5 eV, and the binding energy difference between Fe2p_{3/2} and the satellite peak is 6 eV (Fig. 4f), which is consistent with the results of other researchers [3].

3.1.3. BET analysis

The BET analysis of the three adsorbents is presented in Table 1. The specific surface areas of MWNTS, A-MWNTS, and A-MWNTS/Fe were 90.792, 295.361, and 68.773 m² g⁻¹, respectively. The total pore volume were 0.419, 0.490, and 2.678 cm³ g⁻¹. Compared with MWNTS, the specific surface area of A-MWNTS increased, because the surface of activated carbon nanotubes changed. The specific surface area of A-MWNTS/Fe was the lowest. It may be that the surface of A-MWNTS is occupied by nano-iron. Compared with one of other single materials, the adsorption capacity of the material had been effectively improved because the total pore volume of A-MWNTS/Fe had increased more than four times.

3.1.4. Fourier transform infrared characterization

The Fourier transform infrared (FT-IR) of MWNT, A-MWNTS, nano-iron, and A-MWNTS/Fe are compared as shown in Fig. 5. It can be seen that A-MWNTS/Fe retains the characteristic peak of A-MWNTS and nano-iron. The characteristic peaks of A-MWNTS and nano-iron in A-MWNTS/Fe did not change significantly before and after loaded, indicating that the loaded process did not destroy their skeleton structure. The peak at 619 cm⁻¹ (A-MWNTS/Fe and Fe) corresponds to the combination of iron and surrounding oxygen ions [37], which corresponds to the Fe–O stretching vibration and deformation vibration, respectively. There is no obvious displacement of the characteristic peak of nano-iron before and after loaded, which proves that the structure of nano-iron before and after loaded has not changed [38]. The FTIR of A-MWNTS/Fe before and after EE2 adsorption were compared. There was no significant change in the peak of Fe–O contraction vibration, which proved that EE2 removal was an adsorption process.

3.2. Adsorption experiments

3.2.1. Evaluation of removal effect of three adsorbents

In order to evaluate the removal effects of three adsorbents, Fig. 6 presents the removal rate of EE2 by MWNTS,

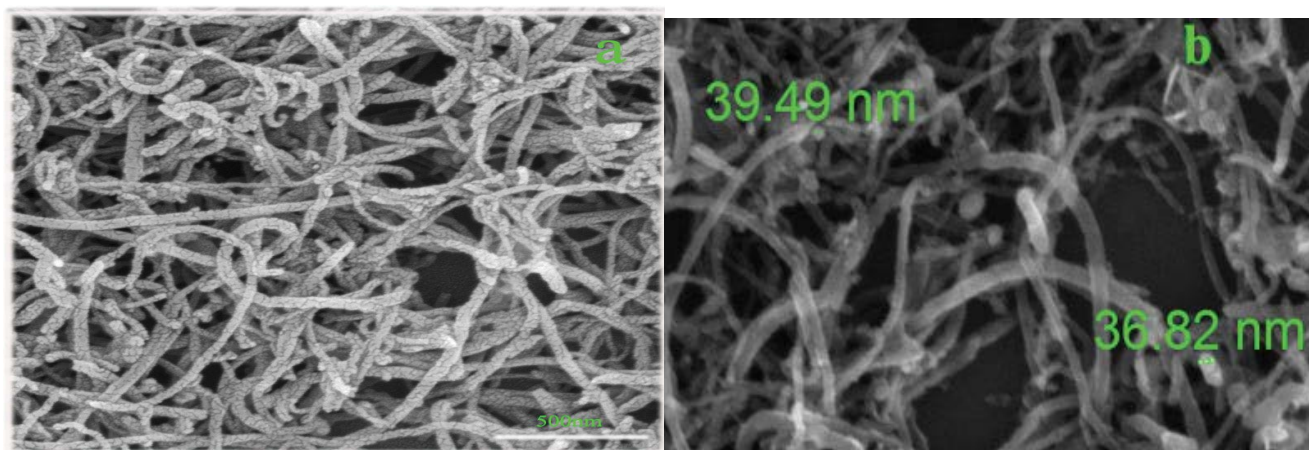


Fig. 3. SEM of A-MWNTS, A-MWNTS/Fe (a) A-MWNTS and (b) A-MWNTS/Fe.

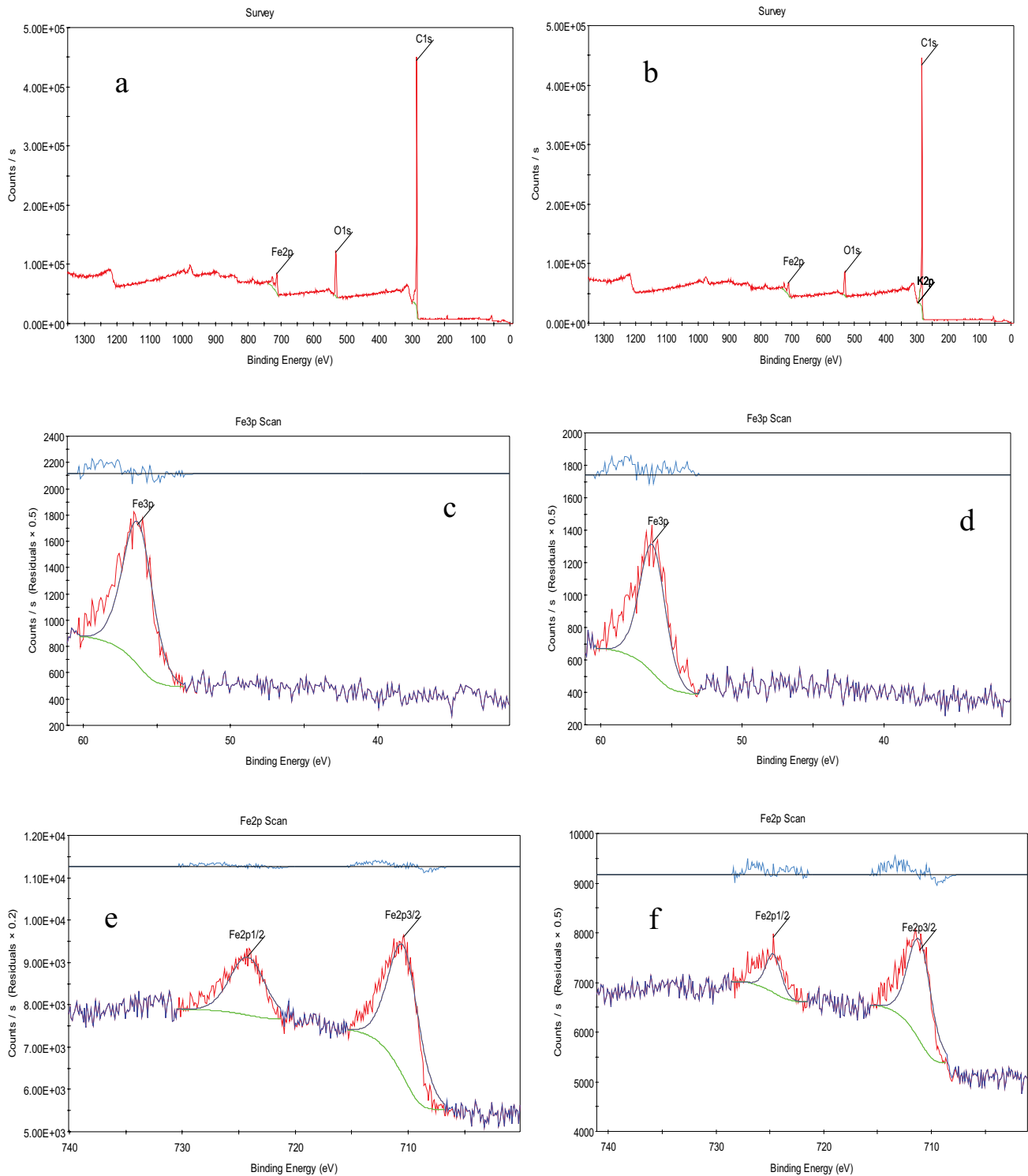


Fig. 4. XPS full scan spectrum before adsorption (a) and after adsorption (b), Fe3p spectrum before adsorption (c), after adsorption (d), Fe2p spectrum before adsorption (e), and after adsorption (f).

Table 1
BET analysis of MWNTS, A-MWNTS, and A-MWNTS/Fe

Sample specific	Surface area (m ² ·g ⁻¹)	Micropore specific surface area (m ² ·g ⁻¹)	Total pore volume (cm ³ ·g ⁻¹)	Pore volume (cm ³ ·g ⁻¹)	Micropore volume (cm ³ ·g ⁻¹)	Average pore width (nm)
MWNTS	90.792	95.509	0.419	0.573	0.037	1.213
A-MWNTS	295.361	290.728	0.490	1.005	0.119	1.264
A-MWNTS/Fe	68.773	74.451	2.678	0.289	0.030	1.407

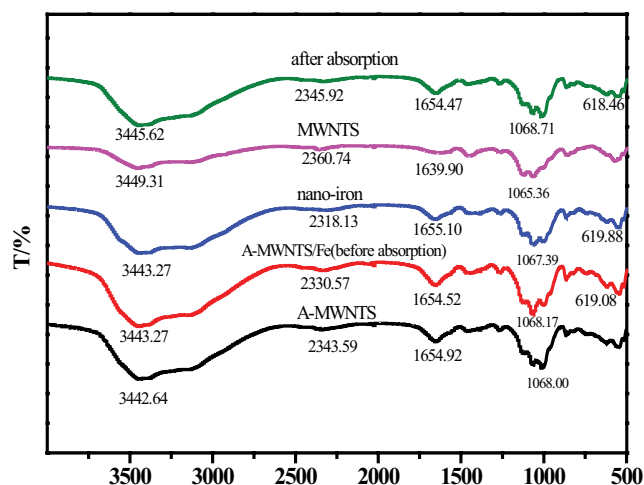


Fig. 5. FTIR spectra of MWNTS, A-MWNTS, Fe, A-MWNTS/Fe, and A-MWNTS/Fe before and after EE2 adsorption.

A-MWNTS, and A-MWNTS/Fe, respectively. It can be seen that the removal rates of EE2 by using A-MWNTS and MWNTS are 86% and 70%, respectively. The removal rate of EE2 by A-MWNTS/Fe can reach 96%. It is further known that the A-MWNTS/Fe composite material has stronger adsorption capacity, which is beneficial to practical applications.

3.2.2. Effect of initial concentration of EE2

The initial concentration of EE2 is an important factor to optimize the adsorption conditions. As exhibited in Fig. 7, C_0 was 3 mg L⁻¹, the removal rate of EE2 was 99%, and the removal rate gradually decreased with the increase of C_0 . When C_0 increased to 9 mg L⁻¹, the removal rate was reduced to 85%. At low concentrations, A-MWNTS/Fe may have more adsorption sites conducive to the rapid adsorption of EE2 [39,40]. With the increase of EE2 concentration, the adsorption capacity of A-MWNTS/Fe will be limited and the removal rate will decrease [41]. Therefore, the optimal initial concentration of EE2 is 3 mg L⁻¹.

3.2.3. Effect of contact time on removal rate

The contact time between the adsorbent and EE2 also has a significant effect on the removal rate. As shown in Fig. 8, the removal capacity of A-MWNTS/Fe drastically increases in the first 20 min. The removal rate of EE2 by A-MWNTS/Fe reached 92% when the removal time was

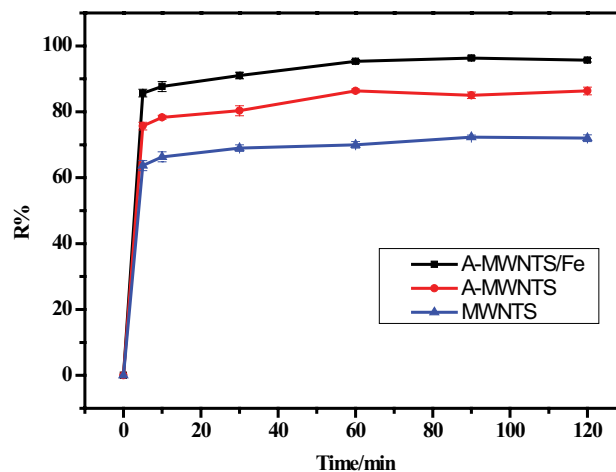


Fig. 6. Effects of different materials on the EE2 removal.

20 min (the point of saturation), and then remained basically stable. These results show that there are plenty of available active sites on the adsorbent surface at the beginning of the experiment, thus facilitating adsorption of EE2. Over time, the active sites are mostly occupied by EE2 until the point of saturation, thereby slowing down the adsorption process beyond the saturation point [42].

3.2.4. Effect of A-MWNTS/Fe dosage

The removal efficiency and adsorption capacity of EE2 are closely related to the dosage of A-MWNTS/Fe. With the increase of the dosage of A-MWNTS/Fe, the removal rate and adsorption capacity of EE2 were gradually increased (Fig. 9). The removal rate reached 95% when the dosage amount reached 0.015 g. Theoretically, as the A-MWNTS/Fe dosage increases, the contact sites of A-MWNTS/Fe and EE2 will increase and the EE2 in the solution is limited, so the removal rate and adsorption capacity of EE2 will remain unchanged. Therefore, the optimum amount of A-MWNTS/Fe is 0.015 g.

3.2.5. pH influence on adsorption process

pH is regarded as a key parameter impacting adsorption capacity. Adjust the pH of the solution with 1 mol L⁻¹ NaOH and 1 mol L⁻¹ HCl. As shown in Fig. 10, under the optimal conditions, the removal rate of EE2 was 63% at pH = 2, and the removal rate of EE2 was 64% at pH = 12. In the pH range of 6–8, the removal rate of EE2 was

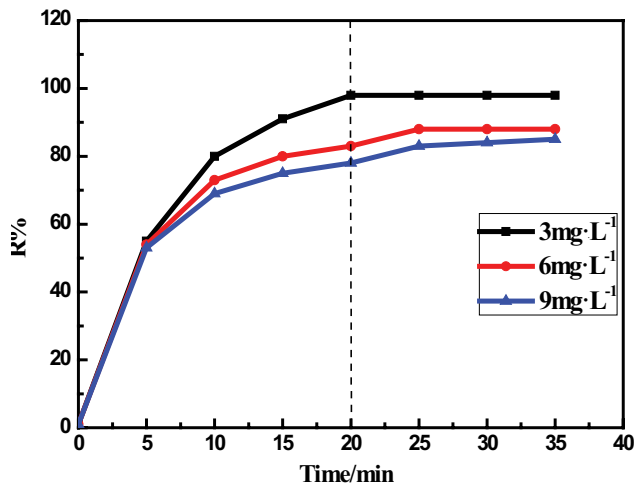


Fig. 7. Effect of initial concentration of EE2.

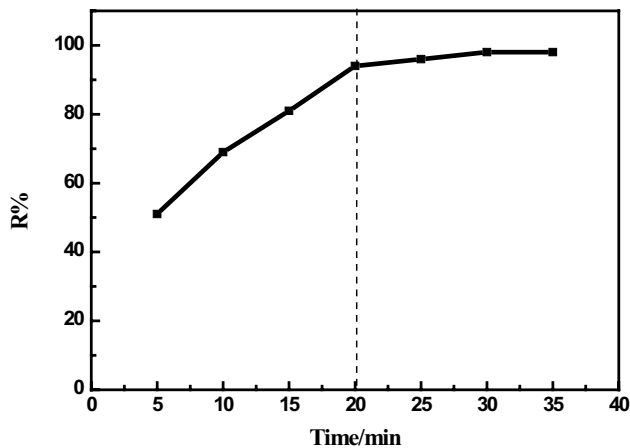


Fig. 8. Effect of time on removal rate.

up to 98%. As the pH value is higher or lower, the removal effect will be suppressed. This may be because further reactions are affected in acidic and alkaline environments [43]. The results show that the adsorption reaction of EE2 is obviously related to pH, and the optimal range is pH 6–8.

3.2.6. Effect of reaction temperature on removal rate

As shown in Fig. 11, the removal rate was consistently reduced with the increase of temperature. At 15°C, 25°C, 35°C, and 45°C, the removal rates of EE2 were 98%, 86%, 79%, and 74%, respectively. In the range of 15°C–25°C, the removal rate was more than 80%. This shows that adsorption can be carried out in a wide temperature range. This suggests that the adsorption process most likely underwent chemical rather than physical action, and the adsorption is beneficial at the lower temperature range [44]. Perhaps this adsorption is an exothermic process, and the increase in temperature leads to a decrease in the removal rate [45]. Therefore, in order to ensure the feasibility of operation, the temperature can be controlled at 15°C–25°C.

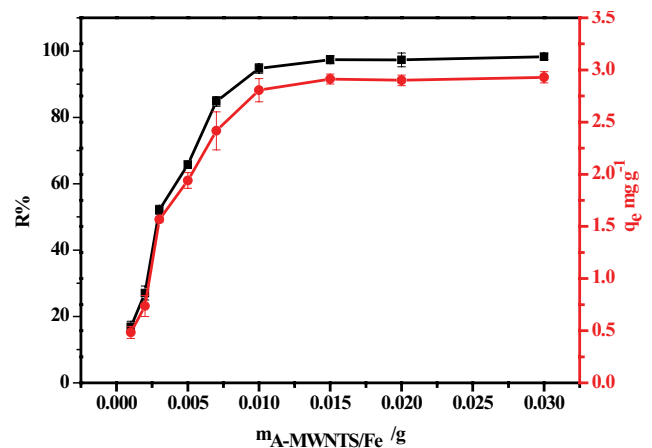


Fig. 9. Effect of A-MWNTS/Fe dosage on removal rate.

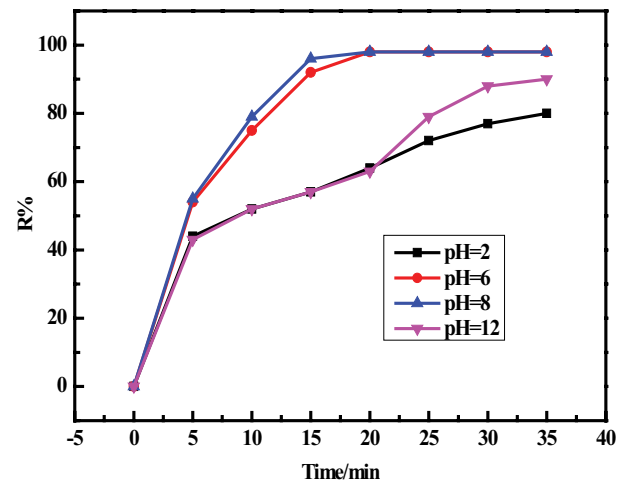


Fig. 10. Effect of different pH on the EE2 removal rate.

3.2.7. Influence of interference factors

Due to the actual application, there are some interfering substances in the actual water, such as common anions (Cl^- , CO_3^{2-}), humic acid, etc. The effects of surfactants, inorganic ions, and organics (such as CTAB, NaCl, CaCl_2 , HAC, CO_3^{2-} , and humic acid) on adsorption were also investigated under optimal treatment conditions. As shown in Fig. 12, the removal rate of EE2 was 98% without interference, and the removal rate of EE2 was more than 90% in the presence of CTAB, NaCl, CaCl_2 , and HAC. When CO_3^{2-} and humic acid were contained in the solution, the removal rate remained above 80%. This results show that CO_3^{2-} and humic acid have little effect on the removal rate of EE2. This is propitious to its application and generalization.

3.2.8. Removal of EE2 from actual water samples

In order to explore the effect of A-MWNTS/Fe on the removal of EE2 in actual water samples, the experimental measurements performed in the laboratory involved the analysis of EE2 removal from water samples extracted from public water resources. These samples came from Yuhua

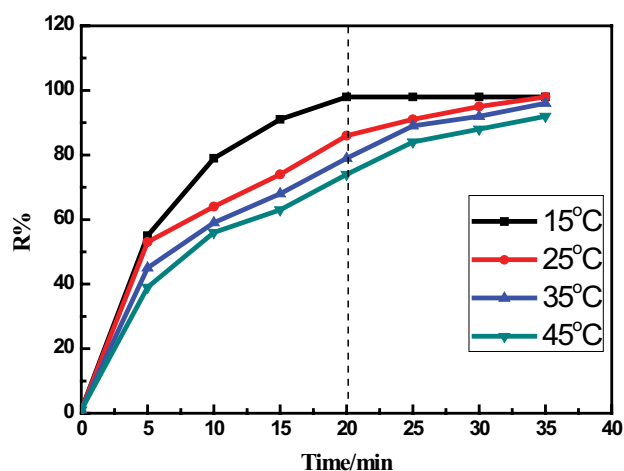


Fig. 11. Effect of temperature on the EE2 removal rate.

Lake, Laoyu River, and a university wastewater treatment plant. Among the three real water samples, only a university wastewater treatment plant detected EE2 with a concentration of 0.47 mg L^{-1} . After removed by A-MWNTS/Fe, the EE2 was completely removed (Table 2). This experimental evidence discloses that A-MWNTS/Fe are qualified for practical application in integrative purification of wastewater polluted by EE2.

3.3. A-MWNTS/Fe regeneration performance evaluation

A good adsorbent should possess high adsorption capacity and good reusability to reduce the total cost. Herein, the A-MWNTS/Fe with saturated adsorption of EE2 was eluted with absolute ethanol and dried for regeneration, and then the regenerated A-MWNTS/Fe material was reapplied to the removal of EE2. As shown in Fig. 13, the removal rate of EE2 could maintain at 88% after three adsorption-desorption cycles. After seven times, the removal rate decreased but still remained at about 70%. This may be the decrease of adsorption sites and reaction activity of A-MWNTS/Fe with the increase of cycle times. The results show that A-MWNTS/Fe has certain recovery value and economic utilization value.

3.4. Comparison of removal properties of similar materials

The endocrine disruptors is mainly removed by the method of microbial treatment, physical adsorption, and chemical method. At present, the removal rate of EE2 in

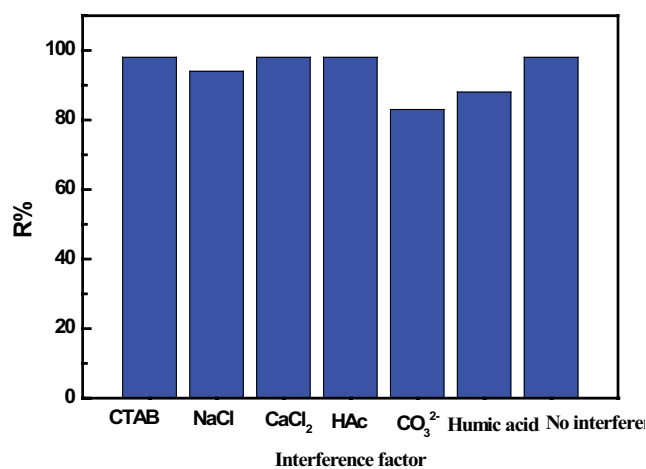


Fig. 12. Effect of interference factors on the EE2 removal rate.

various treatment processes is different, the removal rate is 39.33%–88% [46]. As shown in Table 3, the effect of different materials on the removal rate of EE2 is compared. It can be seen that the removal rate of EE2 by A-MWNTS/Fe is 99%. Obviously, the composite material of this paper has a higher adsorption capacity than other reported adsorbents. In addition, the method is simple in operation, low in cost, and of higher economic value. Therefore, the removal of EE2 by A-MWNTS/Fe is of great significance.

3.5. Adsorption kinetics

We calculated the relevant parameters of the adsorption reaction kinetics. The pseudo-first-order and pseudo-second-order models are commonly used to evaluate the adsorption kinetics using the following equations [47]:

$$V = -\frac{d[C]}{dt} = k_{sa} \cdot a_s \cdot C_0 \cdot [C] = k_{obs} \cdot [C] \quad (3)$$

where V is the removal rate of EE2 ($\text{mg L}^{-1} \text{ min}^{-1}$); k_{sa} is the rate constant of the surface area normalized reaction ($\text{min}^{-1} \text{ m}^{-2} \text{ L}$); a_s is the specific surface area of A-MWNTS/Fe ($\text{m}^2 \text{ g}^{-1}$); $[C_0]$ is the initial concentration of A-MWNTS/Fe (g L^{-1}); $[C]$ is the balance concentration of EE2 in the liquid phase (mg L^{-1}); t is the reaction time (min).

The integral of the above formula can be obtained as follows:

$$\ln[C] = \ln[C_0] - k_{obs} \cdot t \quad (4)$$

Table 2
EE2 removal analysis in actual water samples

Water sample	EE2 initial concentration (mg L^{-1})	Residual concentration of EE2 (mg L^{-1})	Removal rate (%)
Yuhua Lake	–	–	–
Laoyu River	–	–	–
A university wastewater treatment plant	0.47	–	100

“–” Undetected.

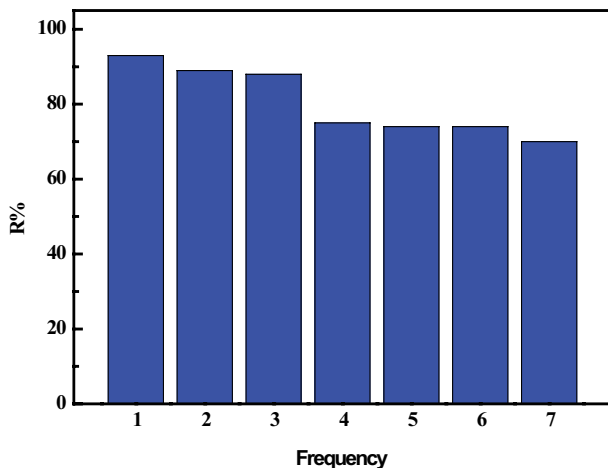


Fig. 13. Evaluation of regeneration performance of A-MWNTS/Fe.

Table 3
Comparison of the maximum removal rate of EE2 by different materials

Material	Removal rate (%)	References
HRP@Fe ₃ O ₄	64.5%	[41]
Algal	60%	[42]
CAS	39%	[43]
Nitrifying bacteria	80%	[44]
A-MWNTS/Fe	99%	This article

$$t_{\frac{1}{2}} = \frac{\ln 2}{k_{\text{obs}}} \quad (5)$$

where $t_{1/2}$ is the half-life (min).

$$\frac{t}{q_t} = \frac{t}{q_e} + \frac{1}{k_2 q_e^2} \quad (6)$$

where q_t (mg g⁻¹) and q_e (mg g⁻¹) are the adsorption capacities of EE2 at time t (min) and equilibrium time (min), respectively, k_2 (g (mg min)⁻¹) is a pseudo-second-order kinetic constant rate constant.

As shown in Table 4 and Fig. 14, the R^2 value of A-MWNTS/Fe is 0.9999, indicating that the adsorption process of EE2 by the A-MWNTS/Fe composite material follows the pseudo-secondary model. It proves that

Table 4
Comparison of apparent rate constants for removal of the EE2 removal by three materials

Variable	Pseudo-first-order kinetic			Pseudo-second-order kinetic		
	k_1 (min ⁻¹)	R^2	Equation	k_2 (g·mg ⁻¹ ·min ⁻¹)	R^2	Equation
A-MWNTS/Fe	0.0204	0.9873	$y_1 = 0.61716 - 0.02037x$	0.0181	0.9999	$y_1 = 0.02161x - 0.02586$
A-MWNTS	0.0089	0.9771	$y_2 = 1.15656 - 0.00892x$	0.0396	0.9998	$y_2 = 0.03367x - 0.0286$
MWNTS	0.0034	0.8752	$y_3 = 1.53582 - 0.00336x$	0.0252	0.9999	$y_3 = 0.02952x - 0.03461$

the adsorption capacity of A-MWNTS/Fe for EE2 is better than that of a single material [28].

3.6. Study on adsorption thermodynamics

Many isotherms of adsorption can be used to describe the adsorption of liquid–solid system. The Langmuir and Freundlich isotherm models are the most common.

The linear equations of its isothermal are as follows:

$$\frac{C_e}{q_e} = \frac{1}{q_m K_L} + \frac{C_e}{q_m} \quad (7)$$

$$\ln q_e = \frac{1}{n} \ln C_e + \ln K_F \quad (8)$$

where q_m is the saturated adsorption capacity (mg g⁻¹), q_e is the equilibrium adsorption capacity (mg g⁻¹), K_L is the adsorption coefficient (L mg⁻¹) related to temperature and heat of adsorption and C_e is the concentration of EE2 (mg L⁻¹) in the equilibrium of adsorption where n is an empirical constant related to temperature. It is generally believed that $1/n$ value of 0.1–0.5 indicates that adsorption is easy, while $1/n > 2$ indicates that adsorption is difficult. K_F is Freundlich adsorption coefficient.

According to the Langmuir and Freundlich adsorption isotherm models, the relevant adsorption isotherm parameters were calculated (Table 5). The correlation coefficient R^2 of the Langmuir isotherm model is all greater than 0.9. The Langmuir isotherm model can better characterize the adsorption capacity of A-MWNTS/Fe on EE2. Therefore, EE2 is adsorbed as a monolayer on the surface of A-MWNTS/Fe. Because nano-iron itself has a certain adsorption effect on EE2 [48], and A-MWNTS can enhance the activity of nano-iron to make the iron carbon contact closely. EE2 is easier to enter the surface of A-MWNTS/Fe, thus greatly improving the removal rate of EE2 [49].

4. Conclusion

In this study, a novel material A-MWNTS/Fe for EE2 removal in water was successfully prepared. The A-MWNTS/Fe for the EE2 removal performance was characterized by using TEM, XPS, and BET. Using A-MWNTS as carrier can improve the dispersion of composite materials and increase the active points and effective contact area of A-MWNTS/Fe. When the dosage of A-MWNTS/Fe is 0.015 g and the reaction time is 20 min, the initial concentration of EE2 is 3 mg L⁻¹, the pH is 6–8 and the temperature

Table 5
Langmuir and Freundlich isotherm model parameters

Adsorption model	Parameter	A-MWNTS/Fe		
		298 K	308 K	318 K
Langmuir model	q_m (mg g ⁻¹)	1.3592	1.0771	0.8523
	K_L (L mg ⁻¹)	3.9169	2.4791	1.7803
	R^2	0.9675	0.9560	0.9508
	Equation	$C_e/q_e = C_e/1.3592 - 0.18783$	$C_e/q_e = C_e/1.0771 - 0.3745$	$C_e/q_e = C_e/0.8523 - 0.65834$
Freundlich model	$1/n$	0.6473	0.6398	0.6101
	K_f (mg g ⁻¹)(L mg ⁻¹) ^{-1/n}	1.3669	1.7508	1.7282
	R^2	0.8884	0.9155	0.8634
	Equation	$\ln q_e = 0.6473 \ln C_e - 0.3125$	$\ln q_e = 0.6398 \ln C_e - 0.5601$	$\ln q_e = 0.6101 \ln C_e - 0.5471$

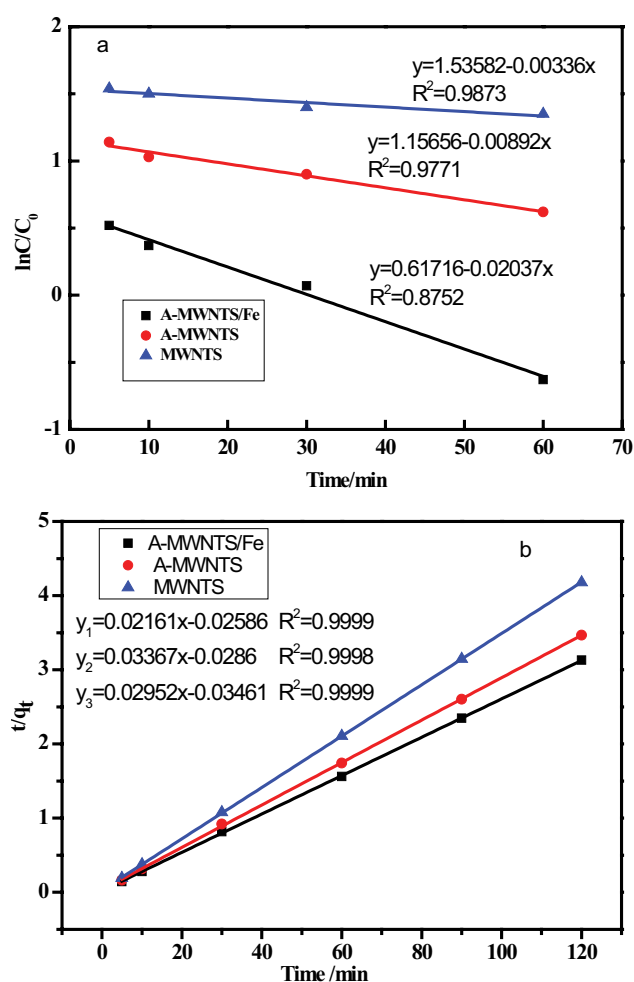


Fig. 14. (a and b) Apparent primary reaction kinetic fitting curves for the EE2 removal by three materials.

is within the range of 15°C–25°C, the EE2 has good adsorption performance and the removal rate can reach more than 99%. In addition, the composite material has good reusability, and the adsorption capacity is maintained at 70% after seven sorbent–desorption cycles. It can be seen that the

A-MWNTS/Fe has excellent recycling value. The adsorption data are found to be more consistent with both pseudo-second-order kinetic models and Langmuir isotherm models. Therefore, A-MWNTS/Fe is an ideal adsorbent for EE2 removal. This study is expected to shed some new light on broader potential applications in environmental research.

Acknowledgments

This work was funded by the National Natural Science Foundation of China (21767030), Yunnan Provincial Department of Education YMU-DEAKIN International Functional Materials Related Laboratory (2017ZZX087), China University Students Innovation and Entrepreneurship Training Program (201610691004), Yunnan Provincial University Students Innovation and Entrepreneurship Training Program 2019, Innovation and entrepreneurship training program for college students of Yunnan Minzu University.

References

- [1] C.B. Vidal, A.V. Feitosa, G.P. Pessoa, G.S.C. Raulino, A.G. Oliveira, A.B. dos Santos, R.F. Nascimento, Polymeric and silica sorbents on endocrine disruptors determination, *Desal. Water Treat.*, 54 (2015) 156–165.
- [2] E.M. Saggiaro, F.P. Chaves, L.C. Felix, G. Gomes, D.M. Bila, Endocrine disruptor degradation by UV/chlorine and the impact of their removal on estrogenic activity and toxicity, *Int. J. Photoenergy*, 2019 (2019) 1–9.
- [3] J. de Rudder, T.V.d. Wiele, W. Dhooge, F. Comhaire, W. Verstraete, Advanced water treatment with manganese oxide for the removal of 17 α -ethynylestradiol (EE2), *Water Res.*, 38 (2004) 184–192.
- [4] P.S. Nasirabadi, E. Saljoughi, S.M. Mousavi, Membrane processes used for removal of pharmaceuticals, hormones, endocrine disruptors and their metabolites from wastewaters: a review, *Desal. Water Treat.*, 57 (2016) 24146–24175.
- [5] Q. Sun, G. Zhu, C. Wang, Z. Yang, Q. Xue, Removal characteristics of steroid estrogen in the mixed system through an ozone-based advanced oxidation process, *Water Air Soil Pollut.*, 230 (2019) 218.1–218.14.
- [6] I. Forrez, M. Carballa, H. Noppe, H.D. Brabander, N. Boon, W. Verstraete, Influence of manganese and ammonium oxidation on the removal of 17 α -ethynylestradiol (EE2), *Water Res.*, 43 (2009) 77–86.
- [7] J.-S. Park, N. Her, Y. Yoon, Ultrasonic degradation of bisphenol A, 17 β -estradiol, and 17 α -ethynyl estradiol in aqueous solution, *Desal. Water Treat.*, 30 (2011) 300–309.

- [8] E.K. Maher, K.N. O'Malley, J. Heffron, H. Jingwan, W. Yin, B.K. Mayer, P.J. McNamara, Removal of estrogenic compounds via iron electrocoagulation: impact of water quality and assessment of removal mechanisms, *Environ. Sci. Water Res. Technol.*, 5 (2019) 956–966.
- [9] B.T.S. Bui, A.-S. Belmont, H. Witters, K. Haupt, Molecular recognition of endocrine disruptors by synthetic and natural 17β -estradiol receptors: a comparative study, *Anal. Bioanal. Chem.*, 390 (2008) 2081–2088.
- [10] L. Jin, L. Chai, L. Ren, Y. Jiang, W. Yang, S. Wang, Q. Liao, H. Wang, L. Zhang, Enhanced adsorption-coupled reduction of hexavalent chromium by 2D poly(m-phenylenediamine)-functionalized reduction graphene oxide, *Environ. Sci. Pollut. Res.*, 26 (2019) 1–12.
- [11] S. He, H. Guo, Z. He, C. Yang, T. Yu, Q. Chai, L. Lu, Interaction of *Lolium perenne* and *Hyphomicrobium* sp. GHH enhances the removal of 17α -ethinyestradiol (EE2) from soil, *J. Soil Sediments*, 19 (2019) 1297–1305.
- [12] G. Cunha, B.M. de Souza-Chaves, D.M. Bila, J.P. Bassin, M. Dezotti, Insights into estrogenic activity removal using carbon nanotube electrochemical filter, *Sci. Total Environ.*, 678 (2019) 448–456.
- [13] H. Yimin, L. Xinqing, F.C. Macazo, G. Matteo, R. Cai, S.D. Minter, Fast and efficient removal of chromium(VI) anionic species by a reusable chitosan-modified multi-walled carbon nanotube composite, *Chem. Eng. J.*, 339 (2018) 259–267.
- [14] K.V.G. Ravikumar, G. Debayan, P. Mrudula, N. Chandrasekaran, M. Amitava, *In situ* formation of bimetallic FeNi nanoparticles on sand through green technology: application for tetracycline removal, *Front. Environ. Sci. Eng.*, 14 (2020) 16.
- [15] T.H. Nam, K. Goto, Y. Shimamura, Y. Inoue, T. Hashida, Effects of high-temperature thermal annealing on properties of aligned multi-walled carbon nanotube sheets and their composites, *Compos. Interfaces*, 11 (2019) 1–18.
- [16] Z.L. Cui, L.F. Dong, Z.K. Zhang, Oxidation behavior of nano-Fe prepared by hydrogen ARC plasma method, *Nanostruct. Mater.*, 5 (1995) 829–833.
- [17] C. Ji, L. Meng, H. Wang, Enhanced reductive dechlorination of 1,1,1-trichloroethane using zero-valent iron-biochar-carrageenan microspheres: preparation and microcosm study, *Environ. Sci. Pollut. Res. Int.*, 26 (2019) 30584–30595.
- [18] S. Wu, T. Cajthaml, J. Semerad, A. Filipová, M. Klementova, R. Skala, M. Vitkova, Z. Vařková, M. Teodoro, Z. Wu, D. Martínez-Fernández, M. Komárek, Nano zero-valent iron aging interacts with the soil microbial community: a microcosm study, *Environ. Sci.: Nano*, 6 (2019) 9081–9090.
- [19] Y. Wu, X. Chen, Y. Han, D. Yue, X. Cao, Y. Zhao, X. Qian, Highly efficient utilization of nano-Fe(0) embedded in mesoporous carbon for activation of peroxydisulfate, *Environ. Sci. Technol.*, 53 (2019) 9081–9090.
- [20] B. Wang, Y. Wang, Y. Zhou, F. Qi, Q. Ding, J. Li, X. OuYang, L. Liu, Multi-walled carbon nanotube-reinforced boron carbide matrix composites fabricated via ultra-high-pressure sintering, *J. Mater. Sci.*, 54 (2019) 11084–11095.
- [21] J. Miyamoto, Y. Hattori, D. Noguchi, H. Tanaka, T. Ohba, S. Utsumi, H. Kanoh, Y.A. Kim, H. Muramatsu, T. Hayashi, M. Endo, K. Kaneko, Efficient H_2 adsorption by nanopores of high-purity double-walled carbon nanotubes, *J. Am. Chem. Soc.*, 128(2006) 12636–12637.
- [22] S. Ming-Li, C. Rong-Ming, X. Xue-Cheng, C. Yi-Wei, L. Wei, Adsorption of phenolic compounds on carbon nanotubes, *J. Northeast Normal Univ.*, 36 (2004) 71–75.
- [23] Z. Lei, Study on the Adsorption Behavior of Modified Multi-Walled Carbon Nano-tubes, Central South University, 2013.
- [24] N. Almoisheer, F.A. Alseroury, R. Kumar, T. Almeelbi, M.A. Barakat, Synthesis of graphene oxide/silica/carbon nanotubes composite for removal of dyes from wastewater, *Earth Syst. Environ.*, 3 (2019) 651–659.
- [25] L. Yangmei, Y. Min, T. Wei, Y. Hong-xing, G. Siqu, L. Guizhen, W. Hongbin, Determination of chlorpyrifos, triazophos and profenofos in vegetables by gas chromatography with solid phase extraction using multiwalled carbon nanotubes as adsorbent, *Sci. Technol. Food Ind.*, 35 (2014) 316–320.
- [26] F.H. El-Sweify, I.M. Abdelmonem, A.M. El-Masry, T.E. Siyam, S.F. Abo-Zahra, Adsorption behavior of Co(II) and Eu(III) on polyacrylamide/multiwalled carbon nanotube composites, *Radiochemistry*, 61 (2019) 323–330.
- [27] K. Yang, L.Z. Zhu, B.S. Xing, Adsorption of polycyclic aromatic hydrocarbons by carbon nanomaterials, *Environ. Sci. Technol.*, 40 (2006) 1855–1861.
- [28] H. Zhang, B. Shen, W. Hu, X. Liu, Research on a fast-response thermal conductivity sensor based on carbon nanotube modification, *Sensors*, 18 (2018) 2191.
- [29] S.J. Roosendaal, B.V. Asselen, J.W. Elsenaar, A.M. Vredenberg, F.H.P.M. Habraken, The oxidation state of Fe(100) after initial oxidation in O_2 , *Surf. Sci.*, 442 (1999) 329–337.
- [30] J. Du, Y. Wang, Faheem, T. Xu, H. Zheng, J. Bao, Synergistic degradation of PNP via coupling H_2O_2 with persulfate catalyzed by nano zero valent iron, *RSC Adv.*, 9 (2019) 20323–20331.
- [31] X. Xiaohong, C. Quanshui, Z. Jiawei, L. Xingyu, W. Lingyu, H. Bin, Removal of U(VI) in aqueous solution by supported zerovalent iron on calcium bentonite and the investigation mechanism, *Non-Met. Mines*, 41 (2018) 83–86.
- [32] P. Singh, P. Raizada, S. Kumari, A. Kumar, D. Pathania, P. Thakura, Solar-Fenton removal of malachite green with novel Fe^0 -activated carbon nanocomposite, *Appl. Catal., A*, 476 (2014) 9–18.
- [33] A.M. Puziy, O.I. Poddubnaya, A. Martínez-Alonso, F. Suárez-García, J.M.D. Tascón, Surface chemistry of phosphorus-containing carbons of lignocellulosic origin, *Carbon*, 43(2005) 2857–2868.
- [34] A. Wei, J. Ma, J. Chen, Y. Zhang, J. Song, X. Yu, Enhanced nitrate removal and high selectivity towards dinitrogen for groundwater remediation using biochar-supported nano zero-valent iron, *Chem. Eng. J.*, 353 (2018) 595–605.
- [35] Y.-L. Ge, Y.-F. Zhang, Y. Yang, S. Xie, Y. Liu, T. Maruyamad, Z.-Y. Deng, X. Zhao, Enhanced adsorption and catalytic degradation of organic dyes by nanometer iron oxide anchored to single-wall carbon nanotubes, *Appl. Surf. Sci.*, 488 (2019) 813–826.
- [36] J. Lu, K. Xu, J. Yang, Y. Hao, F. Cheng, Nano iron oxide impregnated in chitosan bead as a highly efficient sorbent for Cr(VI) removal from water, *Carbohydr. Polym.*, 173 (2017) 28–36.
- [37] Y.E. Unsal, M. Soylak, M. Tuzen, Spectrophotometric detection of Rhodamine B after separation-enrichment by using multi-walled carbon nanotubes, *J. AOAC Int.*, 5 (2014) 1459–1462.
- [38] S.M. Ponder, J.G. Darab, T.E. Mallouk, Remediation of Cr(VI) and Pb(II) aqueous solutions using supported, nanoscale zero-valent iron, *Environ. Sci. Technol.*, 34 (2000) 2564–2569.
- [39] H. He, B. Huang, G. Fu, Y. Du, D. Xiong, C. Lai, X. Pan, Coupling electrochemical and biological methods for 17α -ethinylestradiol removal from water by different microorganisms, *J. Hazard. Mater.*, 340 (2017) 120–129.
- [40] X. Feng, X. Ping, J. Wei, W. Dongsheng, Immobilization of horseradish peroxidase on Fe_3O_4 nanoparticles for enzymatic removal of endocrine disrupting chemicals, *Environ. Sci. Pollut. Res.*, 27 (2020) 1–12.
- [41] X. Bai, K. Acharya, Removal of seven endocrine disrupting chemicals (EDCs) from municipal wastewater effluents by a freshwater green alga, *Environ. Pollut.*, 247 (2019) 534–540.
- [42] E. Kassotaki, M. Pijuan, I. Rodriguez-Roda, G. Buttiglieri, Comparative assessment of endocrine disrupting compounds removal in heterotrophic and enriched nitrifying biomass, *Chemosphere*, 217 (2019) 659–668.
- [43] Y. Bin, L. Lina, The influence of temperature on the preparation of single-walled carbon nanotubes by ACCVD, *Technol. Wind*, 17 (2014) 119.
- [44] J. Liu, L. Wan, L. Zhang, Q. Zhou, Effect of pH, ionic strength, and temperature on the phosphate adsorption onto lanthanum-doped activated carbon fiber, *J. Colloid Interface Sci.*, 364 (2011) 490–496.

- [45] B. Geng, Z. Jin, T. Li, X. Qi, Preparation of chitosan-stabilized Fe⁰ nanoparticles for removal of hexavalent chromium in water, *Sci. Total Environ.*, 407 (2009) 4994–5000.
- [46] J. Hu, C. Chen, X. Zhu, X. Wang, Removal of chromium from aqueous solution by using oxidized multiwalled carbon nanotubes, *J. Hazard. Mater.*, 162 (2009) 1542–1550.
- [47] J. Wang, K. Pan, Q. He, B. Cao, Polyacrylonitrile/polypyrrole core/shell nanofiber mat for the removal of hexavalent chromium from aqueous solution, *J. Hazard. Mater.*, 244 (2013) 121–129.
- [48] Q.-H. Zhou, T.-Y. Long, J. He, J.-S. Guo, Removal of BPA and EE2 from water by Mn-Fe embedded in acicular mullite, *Environ. Sci.*, 41 (2020) 763–772.
- [49] S. Yan, Y. Chen, W. Xiang, Z. Bao, C. Liu, B. Deng, Uranium(VI) reduction by nanoscale zero-valent iron in anoxic batch systems: the role of Fe(II) and Fe(III), *Chemosphere*, 117(2014) 625–630.